LASER & PHOTONICS REVIEWS

www.lpr-journal.org

Stable Optical Frequency Comb Distribution Enabled by Hollow-Core Fibers

Zitong Feng, Giuseppe Marra, Xi Zhang, Eric R. Numkam Fokoua, Hesham Sakr, John R. Hayes, Francesco Poletti, David J. Richardson, and Radan Slavík*

Over the last two decades, optical frequency combs (OFCs) have enabled some of the most accurate measurements in physics. Distributing light from OFCs via optical fibers could make these high-accuracy measurement tools available more widely, from a few dedicated metrology laboratories to other laboratories and industry. However, the performance of distributed OFCs is strongly limited by impairments of standard single mode fiber (SMF), most notably its thermal sensitivity of chromatic dispersion, for which no compensation technique has been shown to date. To overcome this limitation, use of a new class of optical fiber is suggested here: a hollow core fiber (HCF), which offers more than an order of magnitude lesser such impairment. The measured OFC frequency stability of the optical mode and mode spacing reaches 1.8×10^{-19} and 1.5×10^{-17} at a few thousand seconds, respectively, after transmitting through 7.7 km of HCF. To the best of knowledge, this is the best ever performance for km-lengths of fiber-based OFC distribution. Besides, other HCF advantages over SMF in this application are discussed. Specifically, HCFs offer over an order of magnitude lower thermal sensitivity of propagation delay, several orders of magnitude lower optical nonlinearity, and almost ten times lower chromatic dispersion.

1. Introduction

Today, optical frequency combs (OFCs) enable some of the world's most precise experiments and are used in many applications, such as comb based spectroscopy[1] and ranging,[2] ultra-low noise frequency synthesis,[3] tests of fundamental physics,[4] and attosecond science.[5] To achieve the best accuracy in these applications, OFCs need to be referenced to a frequency standard, transferring the phase coherence and frequency accuracy of this standard to hundreds of thousands of tones in the optical domain. However, the most accurate frequency standards are realized only in a few dedicated institutions over the world—usually National Metrology Institutes (NMIs). They typically require substantial development effort and cost, a very stable laboratory environment, and specialized personnel to operate them. To enable more widespread use of these standards signal distribution is needed.

The traditional solutions for frequency standard distribution are based on satellite techniques that use either Global Navigation Satellite Systems or geostationary satellites.[6,7] These methods are widely accessible, but provide stabilities at or below 10^{-15}[8] even when averaging over the entire day, a level that is insufficient for comparison and distribution of today's best atomic clocks which can achieve a fractional frequency stability better than 10^{-17}.[9] For better stability, frequency transfer over optical fibers has been widely explored.[10–16] The most commonly used implementation is shown in **Figure 1**a. It involves two OFC sources, one at the end of each fiber link. A continuous-wave (cw) laser is locked to the OFC that itself is referenced to a primary frequency standard, and then transferred through the fiber link. At the user end, the user OFC is locked to this incoming cw signal. The optical path length of the fiber is stabilized to avoid degradation of the cw laser frequency due to any Doppler shift caused by thermally-induced fiber optical path length changes, or due to acoustic pickup. This system occupies only a small fraction of the optical fiber bandwidth, enabling simultaneous transfer of data traffic and the cw reference laser, reducing the cost as only one wavelength channel needs to be rented rather than the entire optical fiber. This method is particularly useful for transfer over long distances (due to the fiber rental cost and because the cw signal is not influenced by fiber chromatic dispersion) and between places that have OFCs and the necessary expertise, for example, to connect NMIs to compare national clocks.[10,13]

The alternative option is to directly distribute the OFC (that typically has broadband spectrum) over optical fibers,[17–21] Figure 1b. One of the advantages of this approach is that users are provided with a frequency standard-referenced OFC source with-

Z. Feng, X. Zhang, E. R. N. Fokoua, H. Sakr, J. R. Hayes, F. Poletti, D. J. Richardson, R. Slavík
Optoelectronics Research Centre
University of Southampton
Southampton SO17 1BJ, UK
E-mail: zitong.feng@soton.ac.uk

G. Marra
National Physical Laboratory
Hampton Road, Teddington TW11 0LW, UK

The ORCID identification number(s) for the author(s) of this article can be found under https://doi.org/10.1002/lpor.202200167

DOI: 10.1002/lpor.202200167

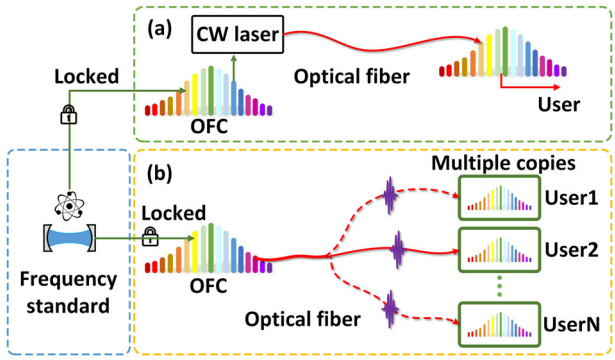

Figure 1. Two approaches to distribute an accurate frequency reference to remote users. a) Synchronizing local and remote OFCs via a cw beam, and b) direct distribution of the OFC via optical fibers.

out requiring frequency metrology skills. One can envisage extending the approach to simultaneously provide a stabilized OFC to many users, where one central OFC laboratory can be used to provide a signal to potentially tens or hundreds of users. Although this will come with some challenges, such as the need to compensate for the fiber transmission loss or coexistence with data traffic sent through the same fiber that may be required to reduce the system cost, they can be overcome thanks to the large transmission bandwidth and low optical nonlinearity of hollow core optical fiber (HCF), as we discuss in detail later. In addition, reliability in this scenario can be straightforwardly improved by having a spare OFC source, which would otherwise (e.g., in Figure 1a) require as many spare OFCs as there are users.

Direct OFC distribution is today used primarily only over very short distances, typically within the walls of one research laboratory. However, a much wider range of applications could be unlocked providing a stable OFC could be reliably distributed over larger distances, **Figure 2**.

For example, an OFC referenced to a frequency standard distributed over < 1 km distances, such as to laboratories within the same or adjacent buildings, can improve resolution via long-time averaging in accurate ranging[22] and spectroscopy,[1] generate ultra-low phase noise and high stability of microwave signal,[23] and stabilize cw lasers at various and user-selectable wavelengths with improved linewidth and frequency stability, Figure 2a.

Stabilized OFC distribution over up to 10 s of km would not require the use of optical amplifiers thanks to the low loss of optical fibers. Remote research laboratories would benefit from such OFC distribution, for example, to enhance the calibration accuracy of spectrographs for astronomy and cosmology[24] or improvement of timekeeping systems.[25] In industry, it could be used, for example, for fast and efficient detection of minute methane emissions from oil and gas fields.[26] In medical diagnostics, OFC distribution could improve sensitivity for identifying small concentrations of a broad range of molecules in the breath, enabling a fast, low-cost screening tool for early warning signs of disease.[27] Although portable OFC systems have been demonstrated, an OFC referenced to a high-stability frequency standard is expected to increase the detected frequency resolution and long-term accuracy.[28,29] Further, it could be used in distributed facilities for large infrastructures or experiments such as arrays of telescopes in astronomy[30] or very long baseline interferometry for geodesy,[31] improves the timing synchronization accuracy, Figure 2b.

As for OFC distribution over distances beyond 10 s of km, it will require optical amplification which will reduce the OFC bandwidth due to the limited amplifier bandwidth, for example, a standard erbium-doped fiber amplifier (EDFA) limits the wavelength range to 1530–1565 nm. However, with new broadband amplifiers emerging (e.g., bismuth-doped fiber amplifiers that have shown promising potential in the 1150–1500 nm and 1600–1800 nm wavelength regions[32]), the long-distance distribution of broadband OFCs will become possible, Figure 2c.

Besides the advantages of the distribution of an OFC locked to a high-quality frequency standard as described above, distribution of an unreferenced OFC could be beneficial in applications such as multi-band radars, as the OFC would enhance the radar performance in terms of sensitivity and resolution simultaneously,[33] and "coherent bridging," that is, wavelength conversion to transfer accurate time and frequency across different parts of a fiber network.[34,35]

It is worth mentioning that distribution of OFC provides versatility over distribution of a single cw laser locked to OFC that is used today. It allows the remote user to, for example, stabilize a cw laser at a wavelength of their choice while simultaneously generating low-noise microwave signals, measure the composition (spectroscopy) and trace (ranging) of the leaking gas at the same time, and synchronize time while simultaneously coherently converting wavelength in a fiber network.

Unfortunately, an OFC signal degrades when propagated through a length of optical fiber. Besides the degradation due to the thermal and acoustic optical path length variations (that also occurs for the aforementioned cw laser frequency transfer), the transfer of an OFC also suffers from fiber chromatic dispersion, and limitations in wavelength bandwidth over which the fiber operates. This makes the transmission of the entire OFC through optical fibers significantly more challenging than for stabilized cw lasers and there is only a very limited number of reports dealing with this topic. Additionally, the transmission of a wide-bandwidth OFC may not allow data channels to be simultaneously transmitted as in the case of the transmission of a single cw stabilized laser (Figure 1a), increasing the operational cost.

In terms of OFC transmission, Marra et al.[21] demonstrated OFC transfer with a bandwidth of ≈90 nm centered around 1550 nm over 7.7 km of standard single-mode fiber (SMF). The fiber optic path length was actively stabilized using a thermally-controlled fiber spool and a PZT fiber stretcher. The thermally controlled spool (300 m of SMF) allowed for compensation of path length changes up to 50 mm in SMF, while the PZT stretcher provided compensation over short time scales. A chromatic dispersion compensating fiber (DCF) of 200 m in length was added to avoid excessive broadening of the OFC pulses in the time domain. This was needed for comparison of the generated OFC pulses and those the full round-trip used for fiber path length stabilization. The achieved fractional frequency stability measured on a single optical mode (around 1542 nm) was 2.1×10^{-18} at a few thousand seconds. However, the stability of the optical modes in other parts of the 90-nm spectrum was not measured. This knowledge is of interest when using OFC in applications such as high precision spectroscopy or when stabilizing multiple lasers at various wavelengths. The mode spacing stabil-

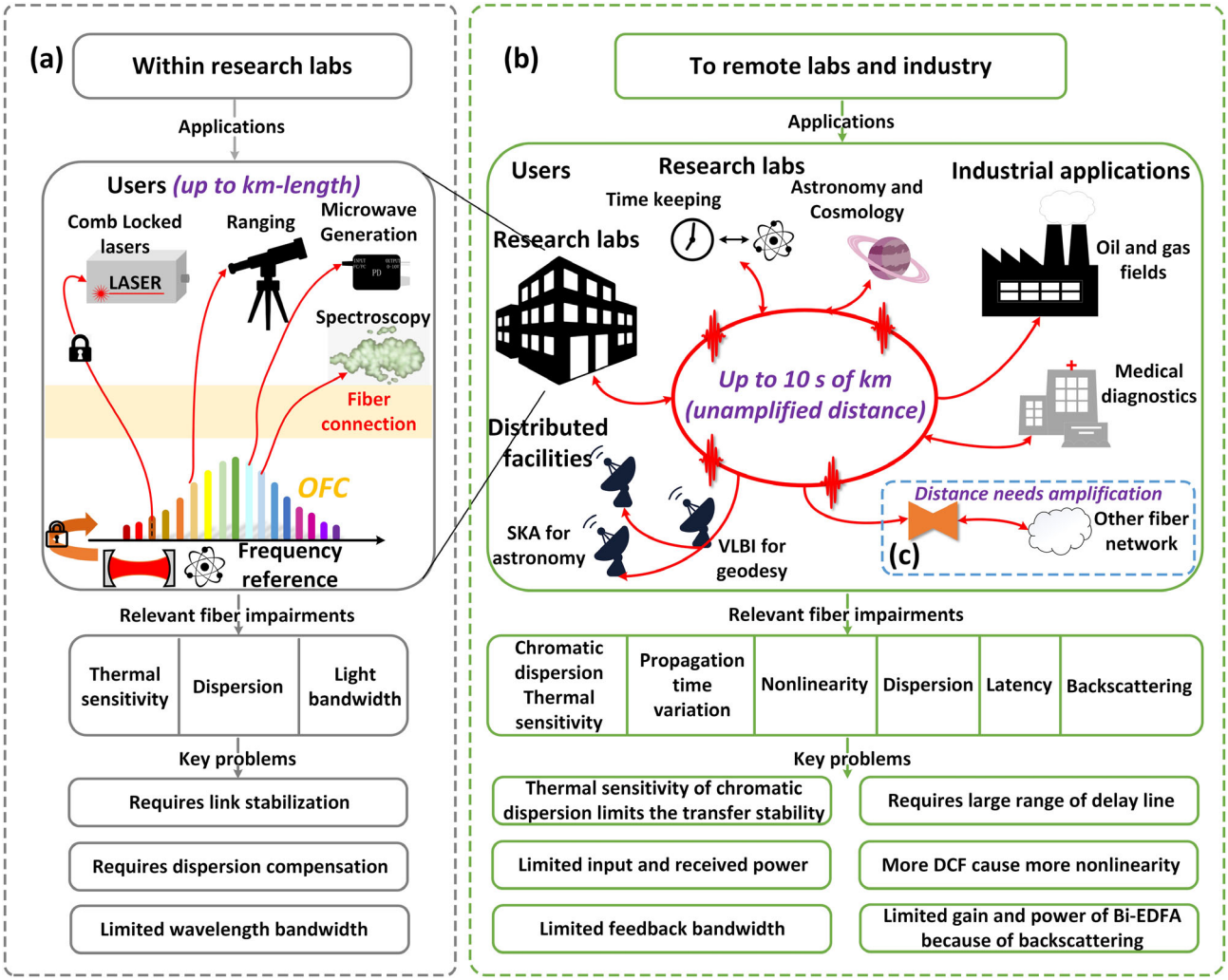

Figure 2. Illustration of the distribution of an OFC through optical fibers for various applications a) within research labs and b) to remote labs and industry. The relevant SMF impairments and associated key challenges and limitations are also shown.

ity after optical-microwave conversion (averaged over the entire 90-nm optical bandwidth) was 4.0×10^{-17} over the same time scale.

In other experiments, OFC light was transferred over longer distances[19] and even through an installed fiber network.[20] However, in these works, the mode spacing stability (transfer of RF signals) rather than the transmission of the optical modes was characterized.

As far as we know, characterization or discussion of the stability of the OFC tones over a spectral range has not yet been discussed in the literature. However, this is a crucial issue for generic OFC dissemination in which some users may require a specific level of stability at various wavelengths or indeed across the entire optical spectrum of the OFC. As we show in this paper, thermally-induced changes in the chromatic dispersion of SMF appreciably degrade the accuracy of the transferred OFC across its extended bandwidth and to the best of our knowledge, no compensation method has been published that can compensate for it. The thermal sensitivity of the chromatic dispersion means that the optical path length change of the fiber is not the same for all optical frequencies. Thus, if the optical path length of the fiber is stabilized at a specific wavelength then spectral components away from this wavelength will not be stabilized to the same extent.

Here we show that using HCF, in place of the SMF, can overcome most of these limitations. In a HCF, the light propagates through the central hole rather than silica glass, giving it many unique properties. The latest generation of HCF has demonstrated an attenuation of 0.174 dB km^{-1},[36] which is already lower than the ordinary SMF (≈0.2 dB km^{-1}) and only slightly above the record-low attenuation of 0.14 dB km^{-1} for the best pure silica core SMF.[37] HCF has already been manufactured in lengths exceeding 10 km, and HCF cables are now commercially-available (e.g., through Lumenisity Ltd[38]). They are already being installed and used to support commercially services in the field, for example, to reduce signal latency in applications such as high frequency trading.[39] More telecom applications are emerging, taking advantage of HCFs large bandwidth, low optical nonlinearity, low and flat chromatic dispersion, and low and stable latency.[40–42] Thanks to the large transmission

bandwidth of HCF, OFC distribution can share the same fiber with telecom data signals to help offset the associated deployment cost. The current bandwidth occupied by data transmission in fiber optic communication systems is around 30 nm (C-band, 1530–1565 nm) to 80 nm (C+L bands, 1530–1610 nm). Fiber attenuation increases rapidly outside of this band, for example, it is 0.4 dB km^{-1} at 1300 nm, which is roughly double that of conventional SMF in the C-band (0.2 dB km^{-1}). HCFs have already been demonstrated with comparable loss to SMF in the C-band (record-low attenuation of 0.174 dB km^{-1}[36]), but lower attenuation at other wavelengths (e.g., 0.22 dB km^{-1} at 1300 nm[36]). This is because the light in HCF propagates through the central core void and as such its attenuation is less influenced by the intrinsic loss of the fiber material. Therefore, it is possible to transmit OFCs with hundreds of nanometers of bandwidth at wavelengths significantly beyond the low-loss (C+L) telecommunication bands. Further, this approach could be exploited over longer distances by using emerging bismuth-doped fiber amplifiers, as discussed previously.[32]

In this work, we demonstrate the transfer of an OFC over a path length-stabilized 7.7 km-long HCF link and compare it to transmission through a 7.5 km path-length stabilized SMF link. We show that the stability of the OFC transmitted degrades significantly less when transmitted through the HCF than the SMF. This is due to many unique HCF features, as we discuss below.

First, it is the low thermal sensitivity of chromatic dispersion in HCF, which we discuss here for the first time and show to be over an order of magnitude lower than in SMF, which is the key to high accuracy OFC transmission in such fibers.

We also demonstrate further advantages of using HCF in this application. First, stabilizing an HCF-based link requires over ten times smaller compensation range. This is due to the HCF delay being over an order of magnitude less sensitive to temperature as compared to the SMF.[43] Further, thanks to the almost ten times lower chromatic dispersion of the HCF with respect to SMF,[44] a significantly shorter length of a chromatic DCF is required for pulse re-compression. This pulse recompression may be necessary, for example, to generate an RF error signal (when returned OFC pulses temporally broaden due to the chromatic dispersion, their temporal overlap with the pulses from the reference OFC is reduced, which may lead to poor signal to noise ratio of the beat signal used for the feedback) for optical path length stabilization of the link.

Transferring an OFC over HCF also offers several additional advantages over SMF, which we do not demonstrate here, but which are expected from HCF performance already discussed in literature: a) the ≈3–4 orders of magnitude lower optical nonlinearity coefficient[45,46] allows for significantly higher powers to be transmitted, enabling more power to be delivered to the users; b) simultaneous low loss, low chromatic dispersion, and low optical nonlinearity over a significantly wider transmission bandwidth of 600–1700 nm[36,45] versus 1200–1700 nm of SMF; c) a 45 dB lower level of backscattered light,[47] which enables higher gains when using bi-directional optical amplifiers without triggering parasitic lasing; d) a 30% lower propagation time (group refractive index is close to 1 for HCF as compared to 1.46 for a typical SMF),[48] reducing the roundtrip time and thus increasing the control-loop bandwidth for optical path length stabilization.

2. HCF and SMF

HCFs have a core with a lower refractive index in the core than the cladding and thus cannot guide light using total internal reflection. There are two main mechanisms for HCF guidance: photonic bandgap[49] and antiresonance.[50] Today, antiresonant HCFs hold the record for the lowest attenuation (0.174 dB km^{-1}[36]), a value comparable to that of SMF in the 1500–1600 nm wavelength range, where SMF attenuation reaches its minimum. Outside of this spectral range, for example, across visible and infrared wavelengths,[36,45] their attenuation is already below that achievable in SMFs. The lowest-loss HCFs reported are of a nested antiresonant nodeless fiber (NANF) or double NANF (DNANF) geometry. Simulations predict that it should be possible to further reduce the HCF attenuation below that of SMFs.[50] Low-attenuation state-of-the-art HCFs theoretically support additional guided modes, however, all these modes have very high attenuation, for example, over 2000 dB km^{-1}, making such fibers "effectively single-mode" after lengths beyond 10 s of meters. Today, these HCFs are commercially available, including cabled HCFs suitable for field deployment.[38]

A number of advantages of low-loss HCF over SMF stem from the reduced light-glass interaction in low-loss HCFs in which the majority of the light propagates in the central core void as opposed to SMF in which light propagates through a glass core. The low-loss HCF's chromatic dispersion is typically around 2–3 ps nm^{-1} km^{-1} over almost entire low-loss transmission window (which can be as large as 600–1700 nm,[36,45]), which is a value almost ten times lower than for SMF in the 1530–1565 nm wavelength range[51] (the lowest-loss telecom C-band). Their optical nonlinearity is reported to be 30–40 dB lower than that of SMF,[45,46] enabling orders of magnitude larger powers to be transmitted without distortion. The propagation time through HCF changes with temperature typically at a rate of 2 ps km^{-1} K^{-1},[43] which is almost 20 times lower than in SMF. Backscattering from the antiresonant HCF microstructure has been shown to be −118 dB m^{-1} at 1550 nm, more than 45 dB lower than SMF.[47] When filled with atmospheric air at atmospheric pressure, back-scattering was predicted to increase to −100 dB m^{-1},[52] which is, however, still ≈30 dB less than for the SMF. The property, which has not previously been discussed in literature and which we show in this article, is the thermal sensitivity of the chromatic dispersion, which is also significantly lower in antiresonant HCFs.

2.1. Fiber Sample Used

For this work, we had a total length of 7.7 km of NANF-type HCF available. The fiber is of a 6 nested element design (a scanning electron micrograph of the core cross section is shown in **Figure 3**a) and operates in the first anti-resonant window. The sample consisted of two lengths of HCF that were 4.3 and 3.4 km long that were spliced together. SMF- pigtails were spliced to each end of the spliced sample to facilitate ready interfacing to SMF-based fiber components, Figure 3b. The average attenuation of the sample was measured to be 0.65 dB km^{-1} at 1550 nm and the total SMF-HCF-SMF loss was 8.8 dB. This is significantly higher than 1.5 dB achievable with current state-of-the-art HCFs and interfacing it with SMF (record-low HCF attenuation pub-

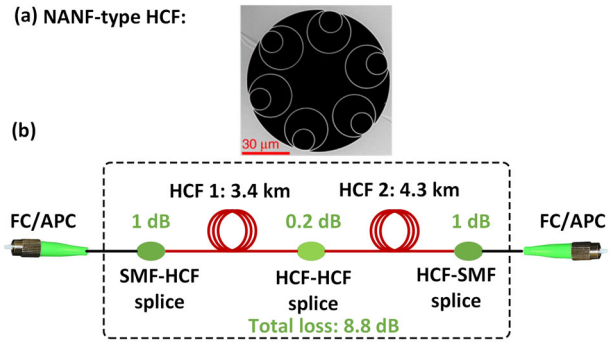

Figure 3. a) Scanning electron micrograph cross section of the used HCF; b) 7.7 km SMF-pigtailed HCF made of two HCF samples.

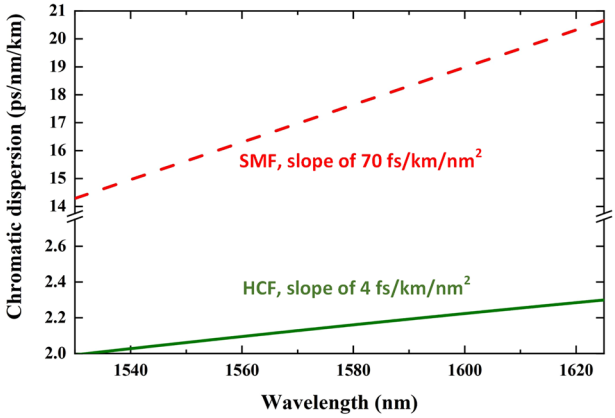

Figure 4. Chromatic dispersion of the HCF (green, solid) and SMF (red, dash) measured over the C+L bands.

lished is 0.174 dB km^{-1}[36] and lowest HCF-SMF connection loss published is 0.10 dB[53]), however, it is still low enough to enable us to demonstrate most of the key HCF advantages for OFC dissemination. The SMF used for comparison was a 7.5 km length of standard SMF-28 fiber with 0.2 dB km^{-1} attenuation at 1550 nm.

2.2. HCF and SMF Thermal Sensitivity of Chromatic Dispersion

The chromatic dispersion thermal sensitivity can be calculated as:[54]

$$\frac{\mathrm{d}D(\lambda)}{\mathrm{d}T} \cong \frac{\mathrm{d}D(\lambda)}{\mathrm{d}\lambda} \cdot \frac{\mathrm{d}\lambda_0(T)}{\mathrm{d}T} = S(\lambda) \cdot \frac{\mathrm{d}\lambda_0(T)}{\mathrm{d}T} \quad (1)$$

where $D(\lambda)$ is the fiber chromatic dispersion (the frequency dependence of the guided mode phase velocity in an optical fiber[55]), $S(\lambda)$ is the chromatic dispersion slope at that wavelength, and λ_0 is the zero chromatic dispersion wavelength. To determine $S(\lambda)$, we measured the chromatic dispersion of the fiber over the C+L telecom bands (see **Figure 4**) using the phase shift method. In this method, a cw tunable laser is modulated and sent through the fiber under test. After photodetection, the phase of this signal, which depends on the fiber group delay, is retrieved. By analyzing its dependence on the laser wavelength, the chromatic dispersion is calculated.[56]

The chromatic dispersion increases linearly with wavelength over the measurement bandwidth. The slope that corresponds to S is then $S = 70$ fs km^{-1} nm^{-2} for SMF and 4 fs km^{-1} nm^{-2} for our HCF. The average chromatic dispersion over the measurement range was $D = 17$ ps nm^{-1} km^{-1} for SMF and $D = 2.2$ ps nm^{-1} km^{-1} for the HCF.

With regards to $\mathrm{d}\lambda_0(T)/\mathrm{d}T$, we used values available in the literature. For SMF, it ranges (at 1550 nm) between 24 and 29 pm K^{-1}.[57,58] In our analysis, we used the minimum value of 24 pm K^{-1}, which should produce the smallest chromatic dispersion thermal sensitivity and thus represents the best-case scenario for the SMF. For the HCF, a change in temperature causes a shift in the transmission window. It has been calculated that this shift is relatively independent of the HCF structure and in the center of the transmission window the value is ≈23 pm K^{-1}.[59] The zero chromatic dispersion wavelength should shift in the same manner, giving $\mathrm{d}\lambda_0(T)/\mathrm{d}T = 23$ pm K^{-1}. The shift in the zero chromatic dispersion wavelength is thus comparable for both, SMF and HCF (23 versus 24 pm K^{-1}). Equation. (1) then suggests that the difference in the thermal sensitivities of chromatic dispersion of the SMF and HCF is mainly due to the different chromatic dispersion slopes. Using the above-discussed numbers in Equation. (1), we obtained chromatic dispersion thermal sensitivity of 1.7 fs nm^{-1} km^{-1} K^{-1} for SMF and 0.1 fs nm^{-1} km^{-1} K^{-1} for our HCF, which is a value more than 17 times lower than for SMF. As we will show later, this value is consistent with our experimental results.

2.3. HCF and SMF Propagation Time Variation

The propagation time variation due to temperature change for SMF and HCF has already been discussed in detail in the literature. There is, however, a range of quoted values. In the SMF, it is mainly due to the different compositions of the fiber core, as the fiber's sensitivity is predominantly given by the core glass thermo-optic coefficient.[43] For the HCF, the variation is mainly due to the fiber coating used,[60] in particular how much it influences the thermal expansion of the fiber, which is the dominant contributor to the HCF's thermal sensitivity. For consistent analysis of our results, we thus first measured the thermal sensitivity of propagation time of our two fiber samples. The two fiber samples are wound on different spools and these were placed as close to each other as possible during the measurements.

Figure 5a shows the experimental set-up for measuring the propagation time variation. As a pulsed source, we used an OFC with 150 fs FWHM pulses at a repetition rate of 250 MHz and spectral width of ≈100 nm (Menlo systems, Germany). We measured the variation of propagation time by measuring the phase difference between harmonics of the repetition rate. To do so, we used a mixer and subsequently converted its output voltage into a time variation. To improve the sensitivity, we measured the 40th harmonic of the repetition rate (10 GHz). This was done by filtering the photodetected signal with a 10 GHz filter which had 3-dB bandwidth of 50 MHz.

Figure 5b shows the fiber path time delay changes when the OFC traveled through the 7.7 km NANF and 7.5 km SMF. The fibers were put in the laboratory environment with the room air conditioner turned on and off every 1000 s, leading to a peak-to-

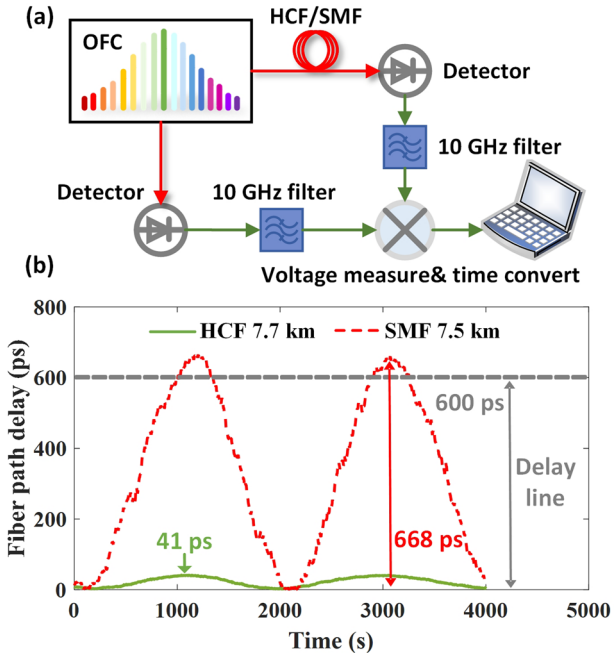

Figure 5. a) Experimental set-up for measuring the propagation time variation in HCF and SMF; b) Fiber path delay change of 7.7 km HCF (green, solid) and 7.5 km of SMF (red, dash) over time when subject to a periodic room temperature variation of 2.25 K. The range of our delay line (600 ps) is shown in grey.

peak temperature change of 2.25 K. Here, we see the SMF exhibited a peak-to-peak time delay deviation of almost 670 ps, while for HCF, the maximum time delay variation was only 41 ps. The measured values correspond to coefficients of thermal delay of 2 and 40 ps km^{-1} K^{-1}, indicating around 20 times temperature sensitivity reduction in HCF in comparison with the SMF, in line with our previously published results.[43]

The 20 times reduction of propagation time temperature sensitivity is important from the practical point of view for OFC transmission, as the methods capable of compensating large optical path length variations cannot be used when transferring an OFC. For example, the most popular method for cw laser transmission uses an acousto-optic modulator (AOM) to shift the cw laser carrier frequency to compensate for the Doppler shift due to the optical path length variations. However, different wavelengths would require different frequency shifts, as accumulated phase depends on the signal wavelength, meaning this method may not provide sufficient compensation over the entire spectral range. Delay line techniques capable of accommodating an entire OFC include thermally-controlled spools and free-space delay lines. Unfortunately, when a large delay (>10 s of cm) is needed they tend to be bulky, heavy, and costly, as large translation stages or long lengths of fiber are required.

The free space delay line we used for compensation of temperature-induced propagation time variation produced a relatively large delay of up to 600 ps, which corresponds to 18 cm in free space. As follows from Figure 5b, this was not sufficient for compensating the SMF link, despite the limited temperature variation experienced in an air-condition-controlled laboratory and relatively modest length. For NANF, the same delay line could even compensate 20 times longer link (120 km), or the same link over significantly larger temperature variations (36 K). which represents more realistic scenarios in terms of lengths and temperature variations.

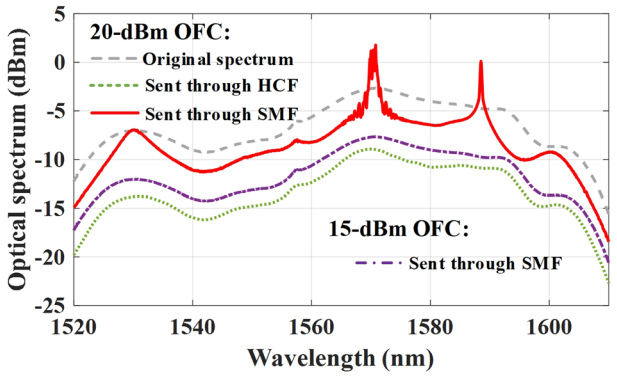

Figure 6. 20-dBm OFC optical spectrum (grey, dash) transmitted through 7.7 km of HCF (green, dot) and 7.5 km of SMF (red, solid). 15-dBm OFC transmitted through SMF (violet, dash-dotted).

2.4. HCF and SMF Power Handling

HCFs can handle significantly larger powers than SMF, for example, over 1 kW average cw[61] (over 4 orders of magnitude higher than for a 1-km long SMF), or over 70 W for ps-length pulses with 40 MHz repetition rate,[62] has been already demonstrated experimentally. Although we do not fully investigate the benefits of this property in this work, we show how the spectrum already becomes distorted by the limited power handling capability of SMF when launching relatively modest OFC powers (less than 20 dBm) into our SMF sample. As shown in **Figure 6**, we observed three peaks (around 1530, 1570, and 1590 nm) in the transmitted spectrum, which were signatures of undesired nonlinear interactions inside the SMF. Such nonlinearities are expected to increase amplitude and phase noise[63] and thus degrade the transmitted OFC signal. In practice, these nonlinear effects limit the maximum power we could launch into the SMF and consequently also the power available to the end users. Whilst higher optical powers were not available in our experiment, the higher optical nonlinearity threshold of HCF should enable the transmission of significantly higher powers. An ultra-stable OFC with 10 W (40 dBm) output power has already been demonstrated and which the authors claim offers potential power scaling beyond 10 kW.[64] Besides enabling the distribution of a relatively high-power OFC to many users, HCF could be beneficially used in applications like attosecond science,[5] where high power carrier envelope stabilized pulses may need to be transmitted.

3. OFC Transfer over Stabilized Fiber

To quantify the improvements that can be achieved with HCF instead of SMF, we built the stabilized link shown in **Figure 7**. In the sections below we introduce our set-up, we compare the transfer stability achieved using SMF and HCF when the OFC bandwidth is limited to 2 nm to investigate the best performance

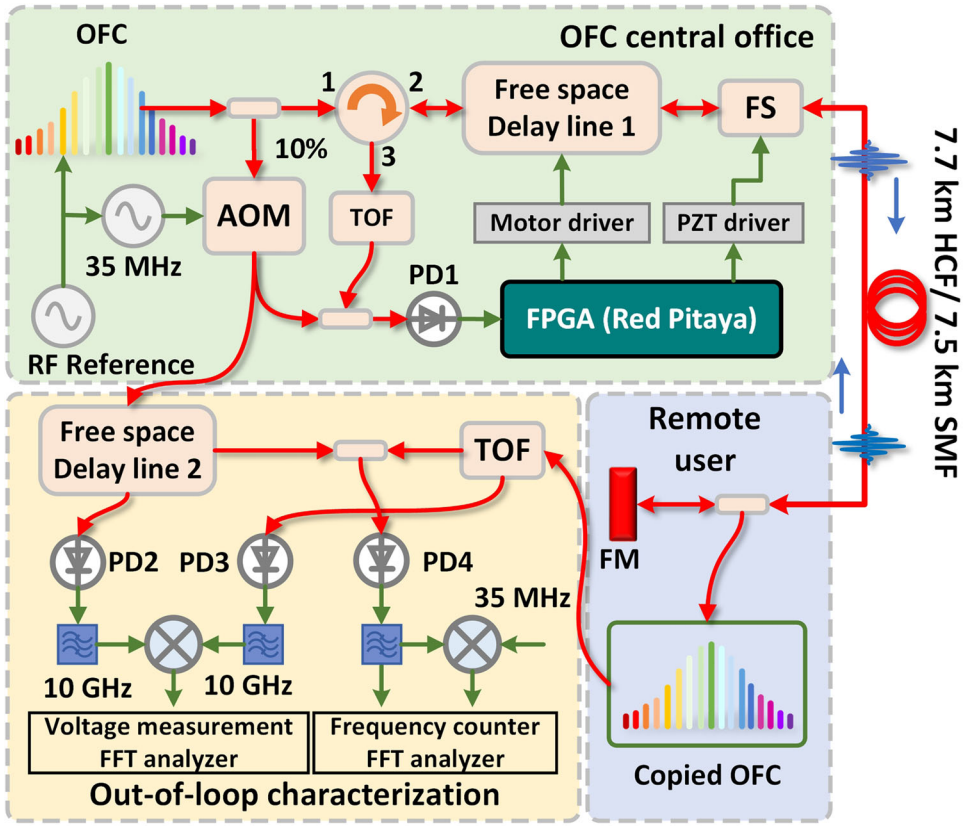

Figure 7. Experimental setup for stabilized OFC transmission consisting of three parts: OFC central office, Remote user, and (out-of-loop) characterization. FS: fiber stretcher; AOM: acousto-optic modulator; TOF: tunable optical filter; FM: Faraday rotator mirror; PD: photo detector.

achievable without any effect related to larger bandwidths such as the thermal sensitivity of chromatic dispersion. Following this, we characterize how the performance is degraded when a larger OFC bandwidth is transmitted.

3.1. Experiment Set-Up

The experimental set-up is shown in Figure 7. The OFC signal was first divided into two parts using a 90/10 coupler. The 10% portion was used as a reference for link noise cancellation and for characterization. Its frequency was shifted by 35 MHz using an AOM frequency shifter. The other 90% of the light was injected into the fiber link after passing through a circulator (that allows for retrieval of the return signal), a free space motor-driven delay line (to compensate for thermally-induced delay and also to overlap the return pulses with the reference pulses), and a fiber stretcher driven by a PZT (to compensate for the relatively fast optical path variations). At the user end, a portion of the signal was tapped out for characterization with the remainder retro-reflected using a fiber-coupled Faraday rotator mirror. The round-trip signal at port 3 of the circulator was filtered with a 30 nm-wide tunable optical bandpass filter. The motivation for using this filter will be explained later. Two proportional-integral (PI) controllers controlled the free space delay line and the fiber stretcher. They were implemented using an FPGA (Red Pitaya, Slovenia) programmed as described in.[65] The delay variation in the fiber pigtails through which the signal does not propagate in both directions (e.g., between the OFC and the AOM) cannot be compensated for and often present a limitation to the overall performance. To minimize this effect, we used as short as possible pigtails in both the measurement and reference path (each with total length less than one meter). We also matched their lengths to within 50 mm to improve the common-mode rejection of environmental effects. Moreover, we put the uncompensated fiber components into a temperature-controlled box (with <50 mK temperature fluctuation) to further reduce their influence on our measurements.

To test the stability, we compared the OFC spacing (repetition rate) and the frequency of selected optical tones between the user end and the transmitter end.

The measurement of the mode spacing stability and phase noise was performed by phase comparison of the 40th harmonic (10 GHz) of the repetition frequency using a microwave mixer. The power spectral density of the phase noise fluctuations between 1 Hz and 100 kHz was measured with an FFT analyzer. The stability was measured by converting the output voltage of the mixer, logged every 1 s with a digital voltage acquisition card, into phase variation.

To measure the frequency stability of the optical mode, we beat the 35-MHz frequency-shifted OFC signal with the OFC signal received at the user end. To temporally overlap the local and remote OFC pulses at the detector we use a second delay line. The power spectral density of the phase noise was measured by

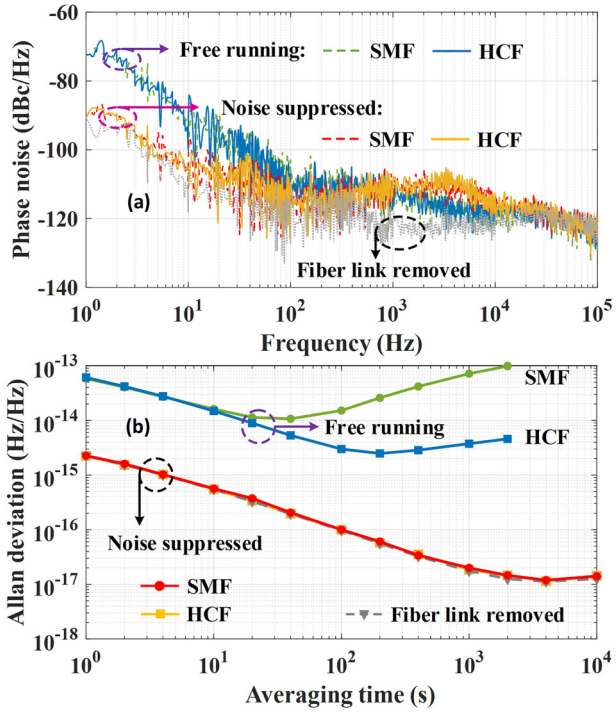

Figure 8. a) Phase noise and b) fractional frequency stability of the 40th harmonic (10 GHz) of the fundamental frequency spacing at the user end.

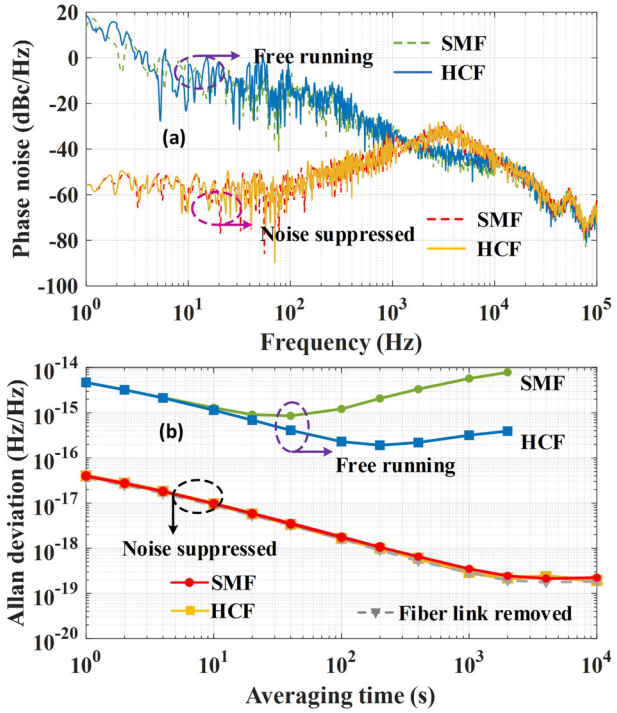

Figure 9. a) Phase noise and b) frequency stability of 1555–1557 nm optical mode at the user end.

mixing the beat frequency with the reference shifted by 35 MHz using an FFT analyzer. The transfer stability was measured by counting the 35 MHz frequency with a digital dead time-free π-type frequency counter.

For SMF, we reduced the optical power sent through the fiber to 15 dBm to avoid the nonlinear effects we described earlier.

3.2. OFC Transmission Performance over a 2 nm Bandwidth

To verify the system performance, we first limited the optical bandwidth used for the link compensation and characterization to 2 nm (1555–1557 nm). This minimizes the degradation due to the fiber chromatic dispersion thermal sensitivity, which we focus on later.

The results including characterization of free-running and optical-path-compensated links with HCF, SMF, and without fiber are shown in **Figure 8**. Both, SMF and HCF links show a similar level of phase noise, Figure 8a, over the entire measurement range when free-running and when noise-suppression is on.

The measured fractional frequency stability characterized by the Allan deviation is shown in Figure 8b. For the free-running link, we see the HCF performs better than SMF, achieving a minimum of 2×10^{-15} (at 200 s averaging time) as compared to 10^{-14} for SMF (at 40 s averaging time). This is expected given HCF's significantly lower thermal sensitivity of propagation time to temperature. For the compensated link, the Allan deviation reached 2.1×10^{-15} at 1 s and 1.5×10^{-17} at 2000 s averaging times for HCF and also for SMF when we removed data points at which the compensation delay line was out of range, as discussed earlier and shown in Figure 5. This performance was identical when the transmitting fiber was removed, suggesting there is no observed degradation of the OFC performance measured due to the propagation through the two fiber samples (HCF and SMF).

The phase noise of the optical modes is shown in **Figure 9**a. Again, both HCF and SMF show the same level of noise for the uncompensated link and also a similar level of phase noise reduction when the phase noise suppression loop is activated. The fractional frequency stability calculated as the Allan deviation from data obtained with the frequency counter is shown in Figure 9b reaching 3.8×10^{-17} at 1 s and 1.8×10^{-19} at 2000 s, which are values close to those obtained when the fiber link was removed.

In all the presented data (RF frequency and optical mode transmission) HCF-based transfer is either similar to that obtained with SMF or better, suggesting there is no penalty in transmitting through HCFs.

3.3. OFC Transmission over a Large Bandwidth

due to the chromatic dispersion thermal sensitivity, we expect the fractional frequency stability of the transferred OFC to be limited. To estimate this effect, we consider a situation in which the temperature changes harmonically (e.g., due to the A/C unit in the laboratory going on and off or day and night) with $2A$ peak-to-peak amplitude and T_1 time period. Then, the Allan deviation $\sigma_y(\tau)$ can be calculated as:

$$\sigma_y(\tau) = \left(\frac{\mathrm{d}D(\lambda)}{\mathrm{d}T} \cdot \mathrm{BW} \cdot L \cdot A\right) \cdot \frac{2}{\tau}\left[\sin\left(\frac{\pi\tau}{T_1}\right)\right]^2 \quad (2)$$

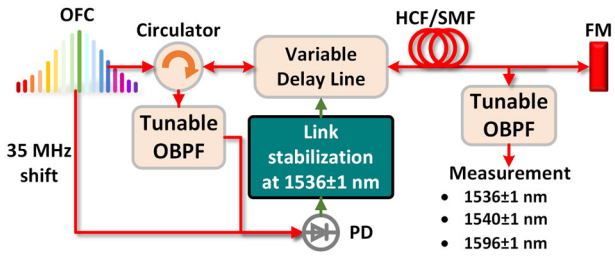

Figure 10. Schematic of the experimental set-up to measure OFC transmission over large bandwidths. OBFP: 2-nm wide optical band-pass filter.

where $dD(\lambda)/dT$ is the coefficient of chromatic dispersion thermal sensitivity described in Equation (1), BWis the wavelength difference between the fully stabilized wavelength and the edge of the transmitted OFC, $L$is the fiber length, and τ is the observation time.

Let us consider the SMF and HCF chromatic dispersion thermal sensitivities calculated in Section 2 and the parameters BW of 4 and 60 nm, $2A = 1.85$ K, and T_1=4000 s (this corresponds to the experimental conditions we show later). Equation (2) then predicts the fractional frequency stability of microwave signal to be limited by 4.7×10^{-17} (SMF) and 3.0×10^{-18} (HCF) at a 4 nm offset and 7.1×10^{-16} (SMF) and 4.3×10^{-17} (HCF) at a 60 nm BW offset, for $\tau = 2000$ s.

To confirm these estimations experimentally, we stabilized the transmission link at 1536 nm (selected via the tunable optical bandpass filter at the OFC end). Subsequently, we measured the OFC transmission performance at wavelengths of 1536, 1540, and 1596 nm (0, 4, and 60 nm from 1536 nm) using the second tunable 2-nm wide optical bandpass filter placed in the user end, as shown schematically in **Figure 10**.

Before performing this experiment, we reduced the laboratory air condition unit output power, which reduced the temperature variations from 2.25 to 1.85 K, so the fiber path delay could always be compensated with our 600-ps delay line, **Figure 11**a.

The result for the three wavelengths is shown in Figure 11b. At 1540 nm ($BW = 4$ nm), the SMF links show a clear degradation, while we observe no degradation when the HCF is used. When a BW of 60 nm is used (1596 nm) we observe a degradation of the stability on both SMF and HCF. However, the HCF degradation is an order of magnitude lower than SMF.

A comparison of the stability measured and predicted (using Equation. (2)) at 2000 s averaging time is shown in **Table 1**. With the exception of the result in HCF for BW = 4 nm, where the measured value was limited by the measurement noise floor, the measured values agree reasonably well with the predictions. Thus, we conclude that Equation. (2) can be used to predict the transfer stability across the transferred frequency spectrum and to estimate the performance with longer HCF and larger temperature changes, which we show in the discussion section. Further, it confirms that the chromatic dispersion thermal sensitivity values we derived earlier are consistent with our measurements.

Finally, the result for optical frequency stability is shown in **Figure 12**. The Allan deviation shows similar trends as for the microwave signal transmission shown in Figure 11. Measurement 60 nm away from the stabilized wavelength (BW = 60 nm), shows

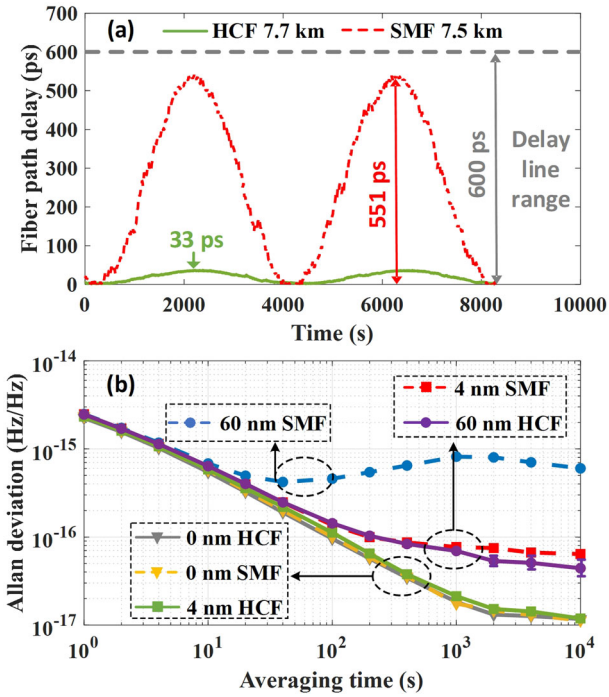

Figure 11. a) Fiber path delay time change of 7.7 km HCF and 7.5 km of SMF with the temperature change of 1.85 K; b) Comparison of the frequency stability of 40th harmonic (10 GHz microwave signal) of the fundamental frequency spacing as affected by the chromatic dispersion thermal sensitivity of HCF and SMF for various levels of BW.

Table 1. Microwave signal fractional frequency stability comparison of OFC distribution through HCF and SMF with 4 and 60 nm BW at averaging time of 2000 s.

BW [nm]	Fiber type	Measured, $\times 10^{-17}$	Predicted, $\times 10^{-17}$
4	HCF	1.5[a)]	0.3
	SMF	7.5	4.7
60	HCF	5.4	4.3
	SMF	80	71

[a)] Limited by the measurement noise floor.

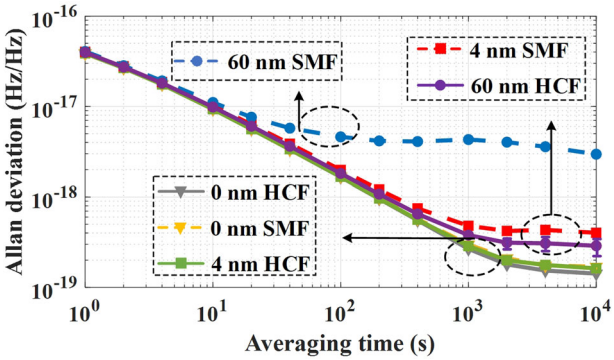

Figure 12. Comparison of the optical frequency stability of HCF and SMF for various levels of BW.

Alan deviation degradation with HCF to be almost one order of magnitude lower than with SMF.

4. Discussion

In this experiment, we demonstrate the transfer of an OFC over 7.7 km HCF and we show that the stability of the OFC, up to 60 nm away from the wavelength used for the optical path length stabilization, is maintained at the level of several parts in 10^{17}. This enables transmission of a 120 nm bandwidth OFC (±60 nm) with this level of stability. Building on these results, we can estimate the stability of practical fiber links, for example, made of an installed fiber and over longer distances. 24-h environmental temperature fluctuation has been reported to be reduced by a factor of 100 when the fiber is installed under 0.5 m of soil.[66] Based on this, we estimate a realistic installed fiber link to have a daily temperature variation of 0.1 K. With such a link, the distribution of a 120 nm wide OFC over 200 km of installed fiber link can maintain frequency stability at the 10^{-18} level (0.1 fs nm^{-1} km^{-1} K^{-1} × 60 nm × 200 km × 0.1 K/86 400 s = 1.4×10^{-18}). This level of stability is sufficient to transfer some of the best frequency standards. For example, the Astro comb locked to Rubidium or Hydrogen atomic clock can be transferred to multiple telescopes which can highly improve the calibration of an astronomical spectrograph to centimeter per second level (This level should make it possible to detect Earth-like planets in the habitable zone of star or even to measure the cosmic acceleration directly).[24] Additionally, this level of stability could in principle enable a timing jitter of 1 ps when transmitting over half-the-globe (20 000 km) (0.1 fs nm^{-1} km^{-1} K^{-1} × 60 nm × 20 000 km × 0.1 K = 1.2 ps), of interest to Earth-size telescopes such as future SKA systems, achieving the same level of timing distribution stability as in the current SKA system.[30]

5. Conclusions

We have demonstrated ultra-stable transfer of OFC derived RF and optical frequencies by replacing the traditional optical fiber used with a glass core with a next-generation optical fiber in which the signal propagates through a central hole (HCF).

These results were enabled by the much lower thermal sensitivity of chromatic dispersion, which we calculated to be 0.1 fs nm^{-1} km^{-1} K^{-1} for our HCF, as compared to the 1.7 fs nm^{-1} km^{-1} K^{-1} of SMF. Our experimental results are consistent with these values, enabling a frequency stability of 5.4×10^{-17} at 2000 s to be achieved over a 60–120 nm OFC bandwidth after propagation through a 7.7 km length of HCF, which is 15 times better than when using a comparable length of SMF (8.0×10^{-16} at 2000 s).

We also showed a transfer frequency stability of the optical modes of 1.8×10^{-19} at a few thousand seconds and of the mode spacing of 1.5×10^{-17} for the same time scale using the HCF which, to the best of our knowledge, is the best fiber-based OFC distribution performance reported so far.

Besides the lower fiber chromatic dispersion thermal sensitivity (which cannot be compensated), HCF has other beneficial features over SMF for the OFC distribution. First, thanks to the lower thermal sensitivity of propagation time a much smaller dynamic range is required of the compensating delay line. Further, its orders of magnitude lower optical nonlinearity enables significantly higher powers to be distributed that can be used, for example, to provide higher power per user, more users, or longer transmission distances (or some combination of the above), Another beneficial feature is the low chromatic dispersion of HCF (approximately eight times lower than SMF at 1550 nm) which results in the need for significantly less dispersion-compensating fiber for re-compression of the OFC pulses in the link noise cancellation loop. In addition, the low HCF backscattering (≈1000 times lower than SMF) may enable higher gain within bi-directional EDFAs than possible with an SMF link. Finally, the 30% higher light propagation speed reduces the signal round-trip time and thus provides for a larger bandwidth for the link noise cancellation feedback loop.

These advantages of HCF over SMF make this novel fiber an ideal candidate for OFC distribution both within the laboratory and indeed to remote external users. This will become of increasing practical interest as HCF becomes more readily available commercially and their attenuation is reduced further toward, and ultimately below, that of SMF.

Acknowledgements

This work was supported by the Engineering and Physical Sciences Research Council (EP/P030181/1), the European Research Council (682724), and the Royal Academy of Engineering.

Conflict of Interest

The authors declare no conflict of interest.

Data Availability Statement

The data that support the findings of this study are openly available in University of Southampton Institutional Research Repository at https://doi.org/10.5258/SOTON, reference number D2306.

Keywords

hollow-core fibers, optical frequency combs, stabilized distribution

Received: March 12, 2022
Revised: June 13, 2022
Published online:

[1] N. Picqué, T. W. Hänsch, *Nat. Photonics* **2019**, *13*, 146.
[2] I. Coddington, W. C. Swann, L. Nenadovic, N. R. Newbury, *Nat. Photonics* **2009**, *3*, 351.
[3] L.-S. Ma, Z. Bi, A. Bartels, L. Robertsson, M. Zucco, R. S., Windeler, G. Wilpers, C. Oates, L. Hollberg, S. A. Diddams, *Science* **2004**, *303*, 1843.
[4] M. Safronova, D. Budker, D. DeMille, D. F. J. Kimball, A. Derevianko, C. W. Clark, *Rev. Mod. Phys.* **2018**, *90*, 025008.

[5] M. Xin, K. Şafak, F. X. Kärtner, *Optica* **2018**, *5*, 1564.
[6] G. Petit, Z. Jiang, *Metrologia* **2007**, *45*, 35.
[7] D. Piester, A. Bauch, L. Breakiron, D. Matsakis, B. Blanzano, O. Koudelka, *Metrologia* **2008**, *45*, 185.
[8] G. Petit, A. Kanj, S. Loyer, J. Delporte, F. Mercier, F. Perosanz, *Metrologia* **2015**, *52*, 301.
[9] N. Hinkley, J. A. Sherman, N. B. Phillips, M. Schioppo, N. D. Lemke, K. Beloy, M. Pizzocaro, C. W. Oates, A. D. Ludlow, *Science* **2013**, *341*, 1215.
[10] J. Guéna, S. Weyers, M. Abgrall, C. Grebing, V. Gerginov, P. Rosenbusch, S. Bize, B. Lipphardt, H. Denker, N. Quintin, *Metrologia* **2017**, *54*, 348.
[11] K. Predehl, G. Grosche, S. Raupach, S. Droste, O. Terra, J. Alnis, T. Legero, T. Hänsch, T. Udem, R. Holzwarth, *Science* **2012**, *336*, 441.
[12] S. Droste, F. Ozimek, T. Udem, K. Predehl, T. Hänsch, H. Schnatz, G. Grosche, R. Holzwarth, *Phys. Rev. Lett.* **2013**, *111*, 110801.
[13] N. Chiodo, N. Quintin, F. Stefani, F. Wiotte, E. Camisard, C. Chardonnet, G. Santarelli, A. Amy-Klein, P.-E. Pottie, O. Lopez, *Opt. Express* **2015**, *23*, 33927.
[14] J. Kim, H. Schnatz, D. S. Wu, G. Marra, D. J. Richardson, R. Slavík, *Opt. Lett.* **2015**, *40*, 4198.
[15] O. Lopez, A. Haboucha, B. Chanteau, C. Chardonnet, A. Amy-Klein, G. Santarelli, *Opt. Express* **2012**, *20*, 23518.
[16] G. Grosche, O. Terra, K. Predehl, R. Holzwarth, B. Lipphardt, F. Vogt, U. Sterr, H. Schnatz, *Opt. Lett.* **2009**, *34*, 2270.
[17] K. W. Holman, D. D. Hudson, J. Ye, D. J. Jones, *Opt. Lett.* **2005**, *30*, 1225.
[18] D. Hou, P. Li, C. Liu, J. Zhao, Z. Zhang, *Opt. Express* **2011**, *19*, 506.
[19] G. Marra, H. S. Margolis, S. N. Lea, P. Gill, *Opt. Lett.* **2010**, *35*, 1025.
[20] G. Marra, R. Slavík, H. S. Margolis, S. N. Lea, P. Petropoulos, D. J. Richardson, P. Gill, *Opt. Lett.* **2011**, *36*, 511.
[21] G. Marra, H. S. Margolis, D. J. Richardson, *Opt. Express* **2012**, *20*, 1775.
[22] K. Minoshima, K. Arai, H. Inaba, *Opt. Express* **2011**, *19*, 26095.
[23] S. A. Diddams, A. Bartels, T. M. Ramond, C. W. Oates, S. Bize, E. A. Curtis, J. C. Bergquist, L. Hollberg, *IEEE J. Sel. Top. Quantum Electron.* **2003**, *9*, 1072.
[24] T. Wilken, G. L. Curto, R. A. Probst, T. Steinmetz, A. Manescau, L. Pasquini, J. I. González Hernández, R. Rebolo, T. W. Hänsch, T. Udem, R. Holzwarth, *Nature* **2012**, *485*, 611.
[25] D. Ludlow, M. M. Boyd, J. Ye, E. Peik, P. O. Schmidt, *Rev. Mod. Phys.* **2015**, *87*, 637.
[26] S. Coburn, C. B. Alden, R. Wright, K. Cossel, E. Baumann, G. W. Truong, F. Giorgetta, C. Sweeney, N. R. Newbury, K. Prasad, I. Coddinton, G. B. Rieker, *Optica* **2018**, *5*, 320.
[27] Q. Liang, Y. C. Chan, P. B. Changala, D. J. Nesbitt, J. Ye, J. Toscano, *Proc. Natl. Acad. Sci. U. S. A.* **2021**, *40*, 118.
[28] B. Bernhardt, A. Ozawa, P. Jacquet, M. Jacquey, Y. Kobayashi, T. Udem, R. Holzwarth, G. Guelachvili, T. W. Hänsch, N. Picqué, *Nat. Photonics* **2010**, *4*, 55.
[29] G. W. Truong, E. M. Waxman, K. C. Cossel, E. Baumann, A. Klose, F. R. Giorgetta, W. C. Swann, N. R. Newbury, I. Coddington, *Opt. Express* **2016**, *24*, 30495.
[30] S. W. Schediwy, in *A Clock for the Square Kilometre Array* (Ed: T. Tzioumis), Vol. *170*, Proceedings of Science, Trieste **2012**, pp. 1–13.
[31] C. Clivati, R. Aiello, G. Bianco, C. Bortolotti, P. De Natale, V. Di Sarno, P. Maddaloni, G. Maccaferri, A. Mura, M. Negusini, *Optica* **2020**, *7*, 1031.
[32] N. K. Thipparapu, Y. Wang, S. Wang, A. A. Umnikov, P. Barua, J. K. Sahu, *Opt. Mater. Express* **2019**, *9*, 2446.
[33] P. Ghelfi, F. Laghezza, F. Scotti, D. Onori, A. Bogoni, *J. Lightwave Technol.* **2016**, *34*, 500.
[34] J. Kim, G. Marra, D. S. Wu, D. J. Richardson, R. Slavík, *Opt. Lett.* **2016**, *41*, 1716.
[35] I. Coddington, W. C. Swann, L. Lorini, J. C. Bergquist, Y. Le Coq, C. W. Oates, Q. Quraishi, K. S. Feder, J. W. Nicholson, P. S. Westbrook, S. A. Diddams, N. R. Newbury, *Nat. Photonics* **2007**, *1*, 283.
[36] G. T. Jasion, H. Sakr, J. R. Hayes, S. R. Sandoghchi, L. Hooper, E. N. Fokoua, A. Saljoghei, H. C. Mulvad, M. Alonso, A. Taranta, T. D. Bradley, I. A. Davidson, Y. Chen, D. J. Richardson, F. Poletti, in *0.174 dB/km Hollow Core Double Nested Antiresonant Nodeless Fibre (DNANF)*, Optica Publishing Group, Washington, DC **2022**, p. Th4C.7.
[37] Y. Tamura, H. Sakuma, K. Morita, M. Suzuki, Y. Yamamoto, K. Shimada, Y. Honma, K. Sohma, T. Fujii, T. Hasegawa, *J. Lightwave Technol.* **2018**, *36*, 44.
[38] Lumensity Ltd., https://lumenisity.com/, (accessed: December 2017).
[39] A. Osipovich, High-Frequency Traders Push Closer to Light Speed With Cutting-Edge Cables, https://www.wsj.com/articles/high-frequency-traders-push-closer-to-light-speed-with-cutting-edge-cables-11608028200, (accessed: December 2020).
[40] A. Nespola, S. Straullu, T. D. Bradley, K. Harrington, H. Sakr, G. T. Jasion, E. N. Fokoua, Y. Jung, Y. Chen, J. R. Hayes, F. Forghieri, D. J. Richardson, F. Poletti, G. Bosco, P. Poggiolini, *J. Lightwave Technol.* **2021**, *39*, 813.
[41] Z. Liu, B. Karanov, L. Galdino, J. R. Hayes, D. Lavery, K. Clark, K. Shi, D. J. Elson, B. C. Thomsen, M. N. Petrovich, D. J. Richardson, F. Poletti, R. Slavík, P. Bayvel, *J. Lightwave Technol.* **2019**, *37*, 909.
[42] Y. Hong, K. R. Bottrill, T. D. Bradley, H. Sakr, G. T. Jasion, K. Harrington, F. Poletti, P. Petropoulos, D. J. Richardson, *Laser Photonics Rev.* **2021**, *15*, 2100102.
[43] R. Slavík, G. Marra, E. N. Fokoua, N. Baddela, N. V. Wheeler, M. Petrovich, F. Poletti, D. J. Richardson, *Sci. Rep.* **2015**, *5*, 15447.
[44] M. Ding, M. Komanec, D. Suslov, D. Dousek, S. Zvánovec, E. R. N. Fokoua, T. D. Bradley, F. Poletti, D. J. Richardson, R. Slavík, *J. Lightwave Technol.* **2020**, *38*, 2423.
[45] H. Sakr, Y. Chen, G. T. Jasion, T. D. Bradley, J. R. Hayes, H. C. H. Mulvad, I. A. Davidson, E. N. Fokoua, F. Poletti, *Nat. Commun.* **2020**, *11*, 6030.
[46] F. Yang, F. Gyger, L. Thévenaz, *Nat. Photonics* **2020**, *14*, 700.
[47] V. Michaud-Belleau, E. N. Fokoua, T. Bradley, J. R. Hayes, Y. Chen, F. Poletti, D. J. Richardson, J. Genest, R. Slavík, *Optica* **2021**, *8*, 216.
[48] F. Poletti, N. Wheeler, M. Petrovich, N. Baddela, E. N. Fokoua, J. Hayes, D. Gray, Z. Li, R. Slavík, D. Richardson, *Nat. Photonics* **2013**, *7*, 279.
[49] F. Poletti, M. N. Petrovich, D. J. Richardson, *Nanophotonics* **2013**, *2*, 315.
[50] F. Poletti, *Opt. Express* **2014**, *22*, 23807.
[51] T. Salgals, A. Supe, V. Bobrovs, J. Porins, S. Spolitis, *Elektron. Elektrotech.* **2020**, *26*, 85.
[52] E. R. Numkam Fokoua, V. Michaud-Belleau, J. Genest, R. Slavík, F. Poletti, *APL Photonics* **2021**, *6*, 096106.
[53] Z. Zhang, W. Ding, A. Jia, Y. Hong, Y. Chen, Y. Sun, S. Gao, S. Huang, Y. Wang, *Opt. Express* **2022**, *30*, 15149.
[54] M. Ding, Z. Feng, D. Marpaung, X. Zhang, M. Komanec, D. Suslov, D. Dousek, S. Zvánovec, E. R. Numkam Fokoua, T. D. Bradley, F. Poletti, D. J. Richardson, R. Slavík, *J. Lightwave Technol.* **2021**, *39*, 2311.
[55] U. Gliese, S. Norskov, T. N. Nielsen, *IEEE Trans. Microwave Theory Tech.* **1996**, *44*, 1716.
[56] E. N. Fokoua, W. Zhu, M. Ding, Z. Feng, Y. Chen, T. D. Bradley, G. T. Jasion, D. J. Richardson, F. Poletti, R. Slavík, *J. Lightwave Technol.* **2020**, *39*, 2142.
[57] M. J. Hamp, J. Wright, M. Hubbard, B. Brimacombe, *IEEE Photonics Technol. Lett.* **2002**, *14*, 1524.
[58] W. Hatton, M. Nishimura, *J. Lightwave Technol.* **1986**, *4*, 1552.
[59] E. R. Numkam Fokoua, M. N. Petrovich, T. Bradley, F. Poletti, D. J. Richardson, R. Slavík, *Optica* **2017**, *4*, 659.

[60] B. Shi, H. Sakr, J. Hayes, X. Wei, E. N. Fokoua, M. Ding, Z. Feng, G. Marra, F. Poletti, D. J. Richardson, R. Slavík, *Opt. Lett.* **2021**, *46*, 5177.
[61] H. C. Mulvad, A. Mousavi, S. Mohammad, V. Zuba, L. Xu, H. Sakr, T. Bradley, J. Hayes, G. Jasion, E. N. Fokoua, A. Taranta, S. Alam, D. J. Richardson, F. Poletti, *Nat. Photonics*, https://doi.org/10.21203/rs.3.rs-1004375/v1.
[62] M. Michieletto, J. K. Lyngsø, C. Jakobsen, J. Lægsgaard, O. Bang, T. T. Alkeskjold, *Opt. Express* **2016**, *24*, 7103.
[63] J. P. Gordon, L. F. Mollenauer, *Opt. Lett.* **1990**, *15*, 1351.
[64] T. Schibli, I. Hartl, D. Yost, M. Martin, A. Marcinkevičius, M. Fermann, J. Ye, *Nat. Photonics* **2008**, *2*, 355.
[65] A. Tourigny-Plante, V. Michaud-Belleau, N. Bourbeau Hébert, H. Bergeron, J. Genest, J.-D. Deschênes, *Rev. Sci. Instrum.* **2018**, *89*, 093103.
[66] T. Pinkert, O. Böll, L. Willmann, G. Jansen, E. Dijck, B. Groeneveld, R. Smets, F. Bosveld, W. Ubachs, K. Jungmann, K. S. E. Eikema, J. C. J. Koelemeij, *Appl. Opt.* **2015**, *54*, 728.